Seismic Waves in Fully Saturated Porous Media: Numerical Modeling

Marcia M. Azeredo (LENEP/UENF), and Viatcheslav I. Priimenko (LENEP/UENF)

Abstract

Through numerical modeling of the theory of poroelasticity, it is possible to compute the seismic and sonic responses of reservoirs saturated by oil and gas and investigate their main characteristics. This work presents numerical simulations of seismic wave propagations in a porous media fully saturated by a viscous fluid. The methodology is based on Ursin's formalism, which derives explicit formulas to the corresponding mathematical problem.

In addition, we performed an analysis of the influence of some important physical parameters such as porosity, permeability, and viscosity.

Introduction

Knowledge of the phenomena associated with the propagation of seismic waves in porous media is fundamental in studying hydrocarbon reservoirs. Modern analysis of these phenomena is based on the theory of poroelasticity developed by Maurice Biot; see (Biot, 1956a, b; Biot, 1962a, b). One of the most important results of this theory is recognizing a second compression wave, called the slow P-wave or slow Biot wave.

Many authors have implemented Biot's theory and compared their results with experimental data; see, for instance, Wyllie et al. (1956), Dutta and Ode (1983), Carcione et al. (2010), and Masson and Pride (2010).

In 1983, Björn Ursin proposed a successful version of the matrix method, which made it possible to obtain analytical expressions for analyzing the propagation of electromagnetic and elastic waves in a three-dimensional space consisting of homogeneous layered layers. Moreover, Ursin's approach allows this method to be applied to systems differential equations, provided that they could be reduced to the so-called Ursin's form; see Ursin (1983) for details.

In this article, we apply the Ursin's formalism to the poroelastic case, when piecewise constant depth functions characterize the physical parameters of the earth's subsurface. Thus, it was possible to solve the problem analytically using the method proposed by Ursin. Moreover, the obtained analytical expressions made it possible to create an efficient mathematical algorithm and fast computer code.

In addition, we carried out a comparative analysis of the influence of some petrophysical parameters, such as porosity, permeability, and viscosity, on the processes of dispersion and attenuation of elastic waves in elastic/porous media. The numerical experiments were carried out both in the reservoir (seismic frequencies) and laboratory (sonic frequencies) scales.

Method

Statement of the problem

Consider wave propagation in a porous half-space $\mathbb{R}^+ = \cup_{k=0}^{n}\mathbb{R}_k$ composed by stratified homogeneous and isotropic layers $\mathbb{R}_k = \{\mathbf{x} = (x,y,z) \in \mathbb{R}^3 : z_k < z < z_{k+1}\}$, where $0 = z_0 < z_1 < \cdots < z_{n+1} = \infty$. All material parameters are represented by piece-wise constant functions depended only on the depth coordinate z, with discontinuities at the internal layer boundaries $z = z_k$, $k = 1,2,\ldots,n$. It is assumed that the wavelength is large in comparison with the dimensions of the macroscopic elementary volume, the displacements both for the fluid and solid phases are small, the liquid phase is continuous, the matrix is elastic and isotropic, and the thermomechanical coupling is absence (Bourbié et al., 1987).

At each point $(\mathbf{x},t) \in \mathbb{R}^+ \times \mathbb{R}_+$, $\mathbb{R}_+ = \{t \in \mathbb{R} : t > 0\}$, the Biot equations of poroelasticity (low-frequency range) are

$$\begin{aligned} \rho\partial_t^2\mathbf{u} + \rho_f\partial_t^2\mathbf{w} &= \nabla\cdot\tau + \mathbf{f}, \\ \rho_f\partial_t^2\mathbf{u} + \rho_w\partial_t^2\mathbf{w} + \frac{\eta}{\kappa}\partial_t\mathbf{w} &= -\nabla p + \mathbf{g} \end{aligned} \tag{1}$$

with the following constitutive relations

$$\begin{aligned} \tau &= (\lambda\nabla\cdot\mathbf{u} + c\nabla\cdot\mathbf{w})\mathbf{I} + \mu\left(\nabla\mathbf{u} + \nabla\mathbf{u}^T\right), \\ p &= -c\nabla\cdot\mathbf{u} - m\nabla\cdot\mathbf{w}. \end{aligned} \tag{2}$$

Vectors $\mathbf{f} = (f_1,f_2,f_3)^T$ and $\mathbf{g} = (g_1,g_2,g_3)^T$ represent the external forces on the porous material and on the pore fluid, respectively. The absolute displacement of the solid phase $\mathbf{u} = (u_1,u_2,u_3)^T$, the relative displacement of the fluid phase $\mathbf{w} = (w_1,w_2,w_3)^T$, the elastic stress tensor τ and the acoustic pressure p are unknown quantities; $\mathbf{I}$ is the 3×3 identity matrix and $(\cdot)^T$ means the transposition of the corresponding quantity.

The material parameters are as follows: λ and μ, the Lamé coefficients, c and m, the Biot moduli, where $c = \alpha m$ (α is the Biot coefficient), ρ, the bulk density, ρ_f, the density of the pore fluid, ρ_w, the effective density, κ, the permeability and η, the pore fluid viscosity. The bulk density ρ is related to the fluid density ρ_f and to the density of the solid material ρ_s through $\rho = (1-\phi)\rho_s + \phi\rho_f$, and the effective density is defined as $\rho_w = a\rho_f/\phi$, where a and ϕ are the tortuosity and porosity of the medium, respectively. According to

Berryman (1980), the tortuosity for spherical solid grains is $a = 1 - 0.5(1 - 1/\phi)$.

At the internal layer boundaries, the functions $\mathbf{u}$, $\mathbf{w}$, p, τ_{13}, τ_{23}, τ_{33} are continuous, i.e.,

$$z = z_k : [\mathbf{u}] = [\mathbf{w}] = \mathbf{0},\ [p] = [\tau_{13}] = [\tau_{23}] = [\tau_{33}] = 0, \quad (3)$$

where $[\cdot]$ means the jump of the corresponding function across the internal layer boundary $z = z_k$; see Carcione (2007). At the free surface $z = 0$, we have the boundary conditions

$$z = 0 : p = \tau_{13} = \tau_{23} = \tau_{33} = 0. \quad (4)$$

Finally, we assume the following initial data

$$t = 0 : \mathbf{u} = \mathbf{w} = \partial_t \mathbf{u} = \partial_t \mathbf{w} = \mathbf{0}. \quad (5)$$

The system (1)–(5) describes the propagation of elastic waves in the porous half-space $\mathbb{R}^+$ composed by stratified homogeneous layers $\mathbb{R}_k$, $k = 1, 2, \ldots, n$.

Dispersion and Attenuation

Elastic waves propagating in a saturated porous medium induce a fluid flow capable of causing dispersion and attenuation through dissipative energy processes. The dispersion and attenuation analysis of this work is based on the formulas obtained in Sharma (2008) and Azeredo and Priimenko (2021).

Analytical Solution

The initial boundary value problem (1)–(5) is solved through the method based on Ursin's formalism (Ursin, 1983); see (Azeredo and Priimenko, 2015, 2021) for more details.

Results

Table 1 gives the physical properties of a homogeneous saturated medium. These data were extracted from Zhu and Mcmechan (1991) and represents the geological model to study the mechanisms of dispersion and attenuation of poroelastic waves.

Table 1: Physical properties of a homogeneous medium.

Property	Symbol	Value
Density of fluid	ρ_f	1000 kg/m^3
Density of solid	ρ_s	2400 kg/m^3
Viscosity of fluid	η	1.0 cP
Porosity	ϕ	0.25
Permeability	κ	400 mD
P-wave velocity on matrix	v_{ps}	2700 m/s
P-wave velocity on fluid	v_{pf}	1500 m/s
S-wave velocity	v_s	1500 m/s

Figure 1 shows the dispersion and inverse of the quality factor (Q^{-1}) curves as a temporal frequency function, where v_{ps}, v_{pf} and v_s are the phase velocities of the fast P-, slow P- and S- waves, respectively. For the low-frequency range, the velocities of S- and fast P- waves are frequency-independent and similar to elastic and poroelastic models, while the slow P-wave is very dispersive (frequency-dependent). At high frequencies, when inertial effects prevail, the dispersion of the slow wave decreases and we can better notice its propagation. The vertical lines represent the critical frequencies f_c (Masson and Pride, 2010).

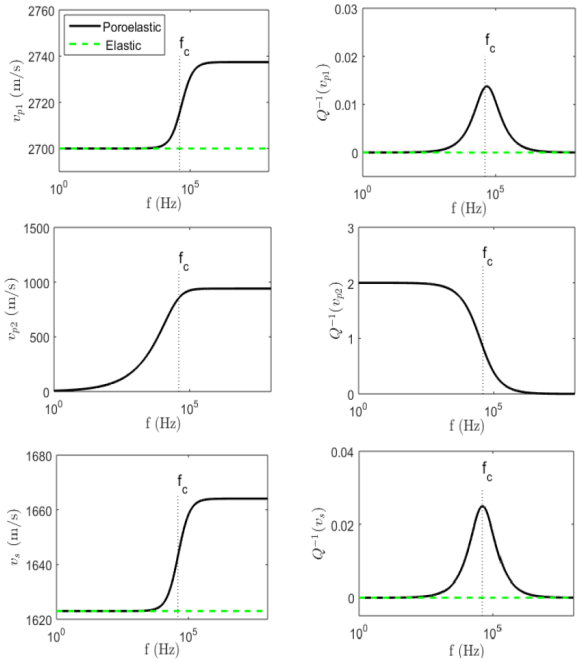

Figure 1: Dispersion and attenuation curves of poroelastic waves.

Figures 2, 3 and 4 show the influence of porosity, permeability and viscosity, respectively, on the propagation of slow wave in a poroelastic medium. The other parameters remain the same as in Table 1. Observe that the phase velocity of the slow wave is not very affected by the porosity in the low-frequency range, whereas, at high frequencies, the porosity influences considerably in the propagation of this wave. Furthermore, an increase in permeability (or decrease in viscosity) results in increased fluid mobility. It is noticed in Figure 3 that as the permeability of the medium increases, the attenuation peak shifts to the high frequencies.

To simulate the elastic wave propagation in a saturated porous medium, we consider a vertical seismic source, represented by the Ricker wavelet pulse, which have the form of the second derivative of the Gaussian function (Ricker, 1953). The numerical experiments occur at the reservoir (seismic frequencies) and laboratory scales (sonic frequencies).

Propagation in a homogeneous medium

Consider a source positioned on the free surface and a receiver at (r, z) coordinates, where r and z are the horizontal and vertical distances between source and receiver (see Fig. 5). For reservoir scale, the dominant frequency of the source is $15\,Hz$, $z = 1000\,m$ and $r = 590\,m$. While for laboratory scale, the dominant frequency is $1.5\,MHz$, $z = 0.01\,m$, and $r = 0.0059\,m$.

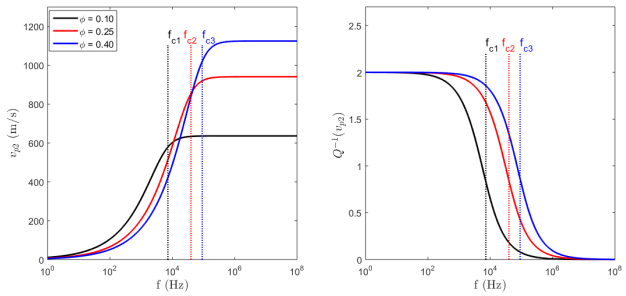

(a) (b)

Figure 2: Dispersion and attenuation of slow wave with variation of porosity.

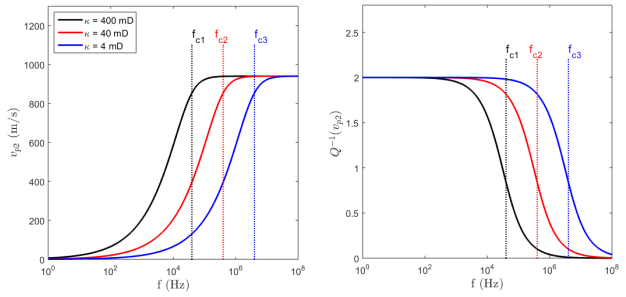

(a) (b)

Figure 3: Dispersion and attenuation of slow wave with variation of permeability.

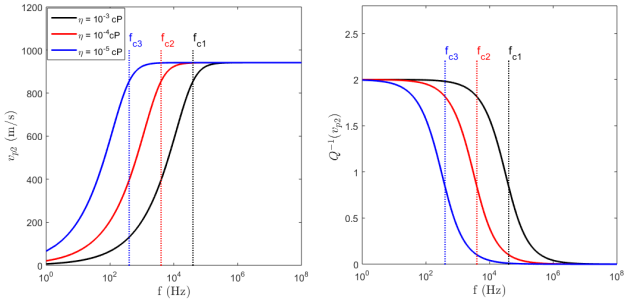

(a) (b)

Figure 4: Dispersion and attenuation of slow wave with variation of viscosity.

We use the following notation: P_{D1} direct fast P-wave, S_D direct shear wave, P_{D2} direct slow P-wave, PP_R reflected fast P-wave, PS_R converted S reflected wave, SP_R converted P reflected wave, and SS_R reflected S-wave.

Figure 6 shows the effect of porosity in the vertical component of fluid relative velocity at the reservoir scale. Observe that, as the porosity increases in the simulations, the amplitude and velocity of the slow P-wave increase too. At low porosity values ($\phi \leq 0.10$), the solid and fluid parts are moving in-phase and the slow wave, which is related to the relative out-of-phase movement, has an extremely small amplitude.

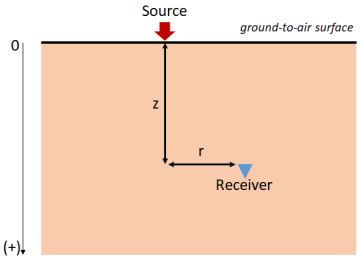

Figure 5: Physical model used in numerical experiments for homogeneous case.

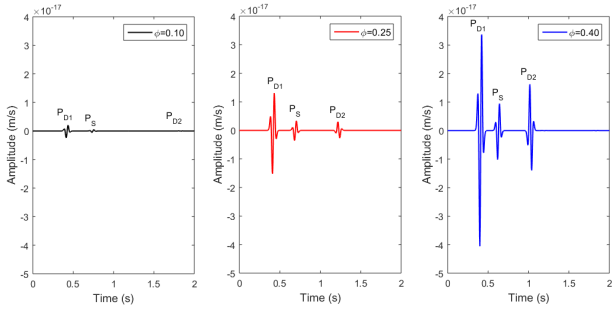

(a) (b) (c)

Figure 6: Vertical component of fluid relative velocity with variation of porosity (seismic frequency)

Figures 7 and 8 show the vertical component of the fluid phase relative velocity in low and high frequencies, respectively, considering three values of permeability. The viscosity of the fluid is fixed at $10^{-9}\,cP$ because the slow P-wave is visible only at small viscosity values (Zhu and Mcmechan, 1991). As the permeability values are reduced, the amplitude of the slow P-wave also decreases. It is noted that, at the sonic frequency, the slow P-wave is observable at lower permeability values than in the case of seismic frequency.

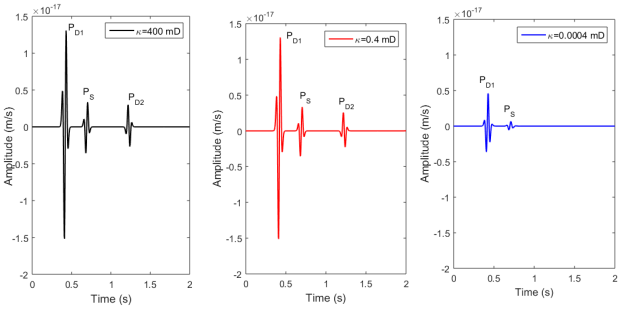

(a) (b) (c)

Figure 7: Vertical component of fluid relative velocity with variation of permeability (seismic frequency)

The effect of viscosity on the wave propagation is shown in Figure 9 (seismic frequencies) and Figure 10 (sonic frequencies), where the notations for direct waves were omitted. Note, in Figure 9, that the slow P-wave is visible

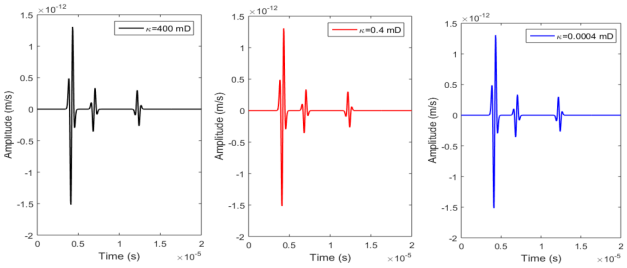

(a) (b) (c)

Figure 8: Vertical component of fluid relative velocity with variation of permeability (sonic frequency)

for viscosities of an order of magnitude less than or equal to about $10^{-5}\,cP$. With the gas viscosity of about $10^{-2}\,cP$, the amplitude of the slow wave was not high enough to be observed under the conditions presented. At the sonic frequencies (Fig. 10), the slow P-wave is observable at higher viscosity values than at the seismic frequencies.

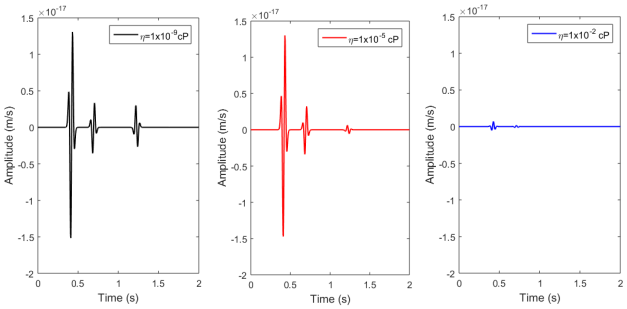

(a) (b) (c)

Figure 9: Vertical component of fluid relative velocity with variation of viscosity (seismic frequency).

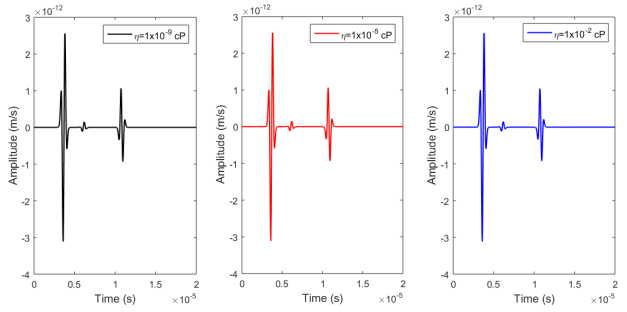

(a) (b) (c)

Figure 10: Vertical component of fluid relative velocity with variation of viscosity (sonic frequency).

Propagation in a heterogeneous medium

As an example, we consider a poroelastic heterogeneous medium modeled by two (Fig. 11a) and three (Fig. 11b) homogeneous horizontal layers whit source on the free surface. For the two layers model (Fig. 11a), the receiver is on the free surface, while for the three layers model, the receiver is at (r,z) coordinates. Moreover, $z=z_1$ and $z=z_2$ are discontinuity surfaces. The physical properties of each layer used in the numerical simulations are listed in Table 2 (Zhu and Mcmechan, 1991).

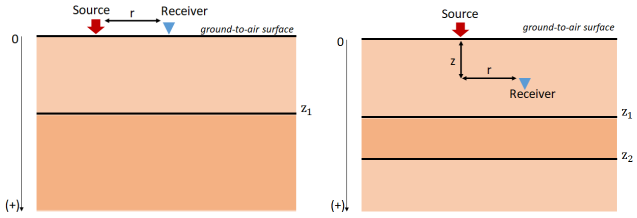

(a) (b)

Figure 11: Physical models of two layers a) and three layers b).

Figures 12 and 13 show traces of the vertical velocity of solid and vertical relative velocity of fluid considering the two layers model (Fig. 11a). We assumed that the first layer in Figure 12 is a water-saturated sandstone while the first layer in Figure 13 is a gas-saturated sandstone (top-down direction); for both, the second layer represents a water-saturated shale.

The dominant frequency of the source is $45\,Hz$, in reservoir scale, and $45\,MHz$, in laboratorial scale. The horizontal distances between source and receiver are $r=150\,m$ and $r=0.15\times10^{-3}\,m$, the first for low frequencies and the last for hight frequencies.

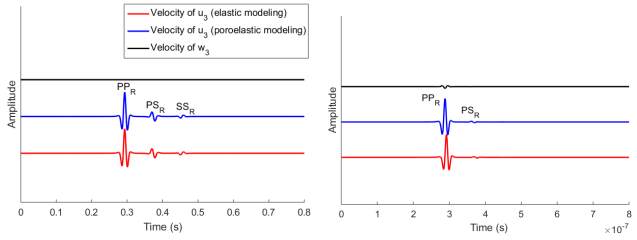

(a) (b)

Figure 12: Vertical components of velocities considering elastic and poroelastic modeling. Water saturated sandstone in the upper layer. Graphics in low a) and high b) frequencies.

Using the matrix velocity (elastic modeling) in high frequencies as a reference, observe that, for the water-saturated medium (Fig. 12b), the relative amplitude of matrix velocity is lower than for the gas-saturated medium (Fig. 13b), as well as the relative amplitude of the fluid relative velocity. This suggests that, at the sonic frequency, in the case of water saturation, a larger part of the poroelastic wave energy propagates in the fluid part and the relative movement between solid and fluid phases (responsible for the attenuation mechanism of Biot's theory) is less than in the case of gas saturation.

The discontinuities of the three layers stratified medium (Fig. 11b) are at $z_1=1000\,m$ and $z_2=1200\,m$. The

Table 2: Physical properties of a heterogeneous medium.

Property	Symbol	Unity	Shale/Water	Sandstone/Gas	Sandstone/Water
Density of fluid	ρ_f	kg/m^3	1000	140	1000
Density of solid	ρ_s	kg/m^3	2413	2630	2630
Viscosity of fluid	η	cP	1.0	2.2×10^{-2}	1.0
Porosity	ϕ	–	0.16	0.25	0.25
Permeability	κ	mD	10^3	10^3	10^3
Velocity of P-wave on solid matrix	v_{ps}	m/s	4790	5450	5450
Velocity of P-wave on fluid	v_{pf}	m/s	1500	630	1500
Velocity of S-wave	v_s	m/s	2520	3250	3250

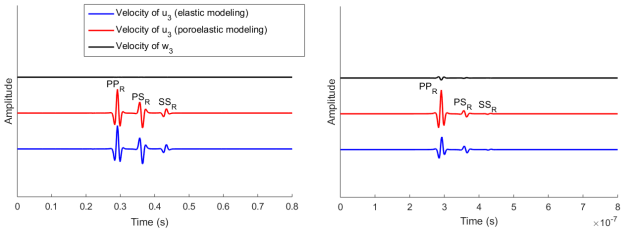

Figure 13: Vertical components of velocities considering elastic and poroelastic modeling. Gas saturated sandstone in the upper layer. Graphics in low a) and high b) frequencies.

source dominant frequency is $25Hz$, and a vertical and horizontal source-receiver distances of $z = 400m$ and $r = 180m$, respectively. The first and third layers simulate water-saturated shale and the second layer simulates a gas-saturated sandstone, according to Table 2. Figure 14 shows the trace of the third component of the solid velocity (poroelastic modeling) in low frequencies. The amplitudes of reflected waves are very small when compared to the amplitudes of direct waves. Therefore, it was chosen to represent in this figure only the reflected waves.

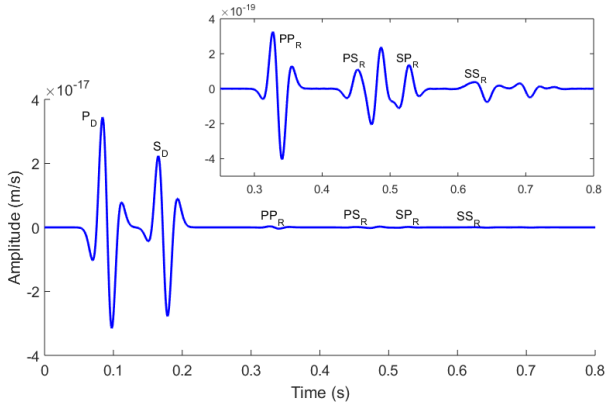

Figure 14: Vertical component of matrix velocity considering poroelastic modeling in low frequencies.

Discussion and Conclusion

In this paper we present some simulation results of elastic wave propagation in heterogeneous porous media approximated by homogeneous and isotropic layers. These results confirm the effectiveness of the matrix method based on the Ursin's formalism.

It was observed that, in the low-frequency range, the slow wave is much more dispersive than the other waves. The velocity of slow wave is affected by porosity and the ratio between viscosity and permeability represents the main influence on the attenuation of this wave.

Simulations for heterogeneous media were performed for poroelastic and equivalent elastic models and were compared to the seismic and sonic frequencies to illustrate the effect of Biot's poroelasticity. This effect was not observed in the simulations at the seismic frequencies, however, it appears significantly at the sonic frequencies. This suggests that this theory can provide valuable results if applied to the inversion of sonic profiles.

References

Azeredo, M. M.; Piimenko, V. I., 2015, An algorithm for wave propagation analysis in stratified poroelastic media, Eurasian Journal of Mathematical and Computer Applications, 3(3), 4–15.

Azeredo, M. M.; Piimenko, V. I., 2021, Numerical Simulation of Seismic Waves in Porous Media, Eurasian Journal of Mathematical and Computer Applications, 9, 4–30.

Berryman, J. G., 1980, Long-wavelength propagation in composite elastic media I. Spherical inclusions, J. Acoust. Soc. Am., 68, 1809–1819

Biot, M. A., 1956a, Theory of propagation of elastic waves in a fluid-saturated porous media. I. Low-frequency range, J. Acoust. Soc. Am., 28, 168–178.

Biot, M. A., 1956b, Theory of propagation of elastic waves in a fluid-saturated porous media. I. Higher frequency range, J. Acoust. Soc. Am., 28, 179–191.

Biot, M. A., 1962a, Mechanics of deformation and acoustic propagation in porous media, Journal of Applied Physics, 33:1482-1498.

Biot, M. A., 1962b, Generalized theory of acoustic propagation in porous dissipative media, Journal of the Acoustical Society of America, 34:1254-1264.

Bourbié, T.; Coussy, O.; Zinszner, B., 1987, Acoustics of porous media. Translation of Acoustique des milieux poreux, Editions Technip, Paris, 1986, 64–65.

Carcione, J. M.; Morency, C.; Santos, J. E., 2010, Computational poroelasticity - a review, Geophysics, 75(5), 229–243.

Dutta, N. C.; Ode, H., 1983, Seismic reflections from a gas-water contact, Geophysics, 48, 148–162.

Masson, Y. J.; Pride, S. R., 2010, Finite-difference modeling of Biot's poroelastic equations across all frequencies, Geophysics, 75(5), N33–N41.

Ricker N., 1953, The form and laws of propagation of seismic wavelets, Geophysics, 18, 10–40.

Sharma, M. D., 2008, Wave propagation in thermoelastic saturated porous medium, J. Earth Syst. Sci., 117(6) 951–958.

Ursin, B., 1983, Review of elastic and electromagnetic waves propagation in horizontally layered media, Geophysics, 48, 1063–1081.

Wyllie, M. R. J.; Gregory, A. R.; Gardner, L. W., 1956, Elastic wave velocities in heterogeneous and porous media, Geophysics, 21(1), 41–70.

Zhu, X.; Mcmechan, G. A., 1991, Numerical simulation of seismic responses of poroelastic reservoirs using Biot theory, Geophysics, 56, 328–339.

Acknowledgments

The authors thank the Leopoldo Américo Miguez de Mello Research Center - CENPES/PETROBRAS for the financial support and the Laboratory of Engineering and Exploration of Petroleum (LENEP/CCT/UENF) for having provided the conditions for this work.